ACS Sustainable Chemistry & Engineering

pubs.acs.org/journal/ascecg

Research Article

Biobased Composites from Eugenol- and Coumarin-Derived Methacrylic Latex and Hemp Nanocellulose: Cross-Linking via [2 + 2] Photocycloaddition and Barrier Properties

Sara Dalle Vacche,* Samantha Molina-Gutiérrez, Giuseppe Ferraro, Vincent Ladmiral, Sylvain Caillol, Patrick Lacroix-Desmazes, Yves Leterrier, and Roberta Bongiovanni

Cite This: *ACS Sustainable Chem. Eng.* 2024, 12, 8741−8751

Read Online

ACCESS | Metrics & More | Article Recommendations | Supporting Information

ABSTRACT: A novel-biobased latex was synthesized by redox-initiated emulsion copolymerization of ethoxy dihydroeugenyl methacrylate with 5 wt % of a photosensitive methacrylate containing a coumarin group. A stable copolymer latex having 16 wt % solids content and a particle size of 53 nm was obtained. The copolymer had a T_g of 29 °C and was soluble in acetone. Coatings were obtained, and the effect of UVA irradiation was tested: the light-induced cross-linking of the copolymer by [2 + 2] cycloaddition of the coumarin pendant moieties was demonstrated by UV−visible spectroscopy. As a consequence of UVA-induced cross-linking, the copolymer became insoluble in acetone. The copolymer latex was combined with hemp-derived nanocellulose to obtain composite self-standing films by simple mixing in an aqueous medium followed by casting, evaporation of water, and hot pressing. The composite films were also successfully cross-linked by [2 + 2] cycloaddition, with an enhancement of barrier properties. The water vapor transmission rate of the cross-linked composite films with up to 45 wt % nanocellulose was 5 times lower than that of the hemp nanocellulose film, while further addition of nanocellulose increased permeability.

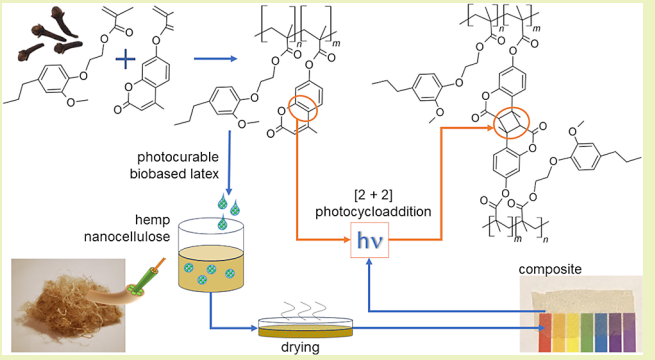

KEYWORDS: *biobased composites, biobased latex, biomass filler, hemp nanocellulose, coumarin, cycloaddition, water vapor barrier*

INTRODUCTION

The use of polymeric materials in several applications enhancing the quality and comfort of modern life has become widespread, although often at the cost of environmental damage and health hazards related to energy-intensive and polluting production processes, exploitation of fossil resources, and incorrect waste disposal habits. The use of renewable resources, including upcycling of waste and valorization of biomass, the adoption of eco-friendly production processes, and the design of new materials coupling durability with sustainable end-of-life options are key strategies for solving these issues.

A great effort is ongoing to enlarge the platform of available biobased raw materials, including those derived from waste biomass through different refining and extraction processes. Cellulose, the most abundant natural polymer, can be extracted in the form of nanocellulose, i.e., nanofibrils or nanocrystals, from a wide variety of lignocellulosic biomasses, including, besides wood, abundant agricultural residues such as rice husks,[1,2] corn stover,[3,4] or hemp stems.[5−7] Nanocellulose shows remarkable mechanical and gas barrier properties in dry conditions, which are however dramatically affected by humid environments.[8] A well-recognized strategy to improve the water resistance of nanocellulose is to combine it with polymers.[9] Among polymeric materials, polymer networks, obtained via thermal or photoinduced cross-linking, offer distinct advantages, such as improved chemical resistance, absence of creep, and durability. Particularly, cross-linking processes induced by light exhibit remarkable energy efficiency and low volatile organic carbon emissions;[10,11] furthermore, the exploitation of renewable carbon[12,13] and the development of photoinitiator-free[14] or reversible[15] reactions are underway for further improving their safety and environmental friendliness.

Due to the polar nature of its molecular structure, rich in surface hydroxyl groups forming inter- and intramolecular hydrogen bonds, nanocellulose tends to aggregate when mixed with nonpolar monomers or oligomers.[16] Complex solvent-mediated procedures or surface modification of nanocellulose

Received: February 16, 2024
Revised: May 14, 2024
Accepted: May 15, 2024
Published: May 30, 2024

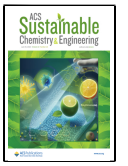

https://doi.org/10.1021/acssuschemeng.4c01365
ACS Sustainable Chem. Eng. 2024, 12, 8741−8751

Scheme 1. Emulsion Copolymerization of EDMA and CouMA

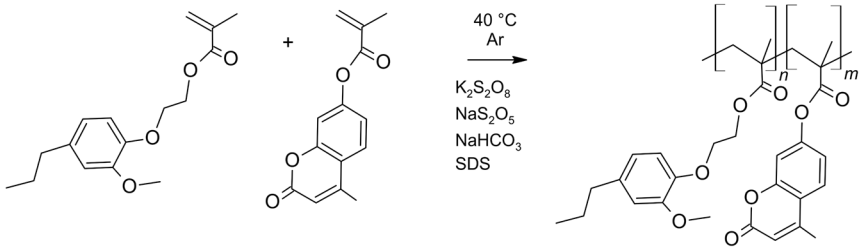

were thus developed to improve dispersion and compatibility with nonpolar polymers.[17] Waterborne polymer latexes offer a simple and environmentally convenient alternative, as they can directly be mixed with nanocellulose in water suspensions. Synthesis of latexes from renewable resources has already been reported in the literature but mainly from vegetable oils, sugars, or terpenes.[18] Although there have been some recent works on cardanol, vanillin, ferulic acid, or eugenol derivatives,[19−22] including those of our team,[23−25] the emulsion polymerization of biobased aromatic monomers remains underdeveloped, in particular the synthesis of aromatic copolymers.

An interesting option for imparting to polymer latexes the ability to form cross-links is the introduction in the polymer structure of moieties able to dimerize upon irradiation with UV light, without the need for photoinitiators. Coumarin, a natural aromatic compound that can be extracted from several plants[26] dimerizes via a photochemical [2 + 2] cycloaddition. This reaction, known since the early 1900s,[27] has in the last few decades been engineered in polymers to prepare light-responsive networks.[28] Some works reported the photo-cross-linking of polymer latex particles exploiting coumarin functional groups, introduced by copolymerization or postpolymerization functionalization.[29,30] Self-healing photoresponsive cellulose nanocrystal-modified fluorinated polyacrylates containing coumarin derivatives were synthesized by Pickering emulsion polymerization.[31−33] In addition, a few examples of partially biobased photoresponsive polymer networks with coumarin functional groups have been reported.[34,35] However, to the best of our knowledge, coumarin-containing biobased polymer latexes photo-cross-linkable via [2 + 2] photocycloaddition have not been widely investigated so far.

In a previous work, we proposed the synthesis of a copolymer latex of ethoxy dihydroeugenyl methacrylate (EDMA) with 1 wt % coumarin methacrylate (CouMA) by redox-initiated emulsion polymerization; the latex was used to prepare composite films reinforced with wood-derived microfibrillated cellulose (MFC), whose oxygen permeability was investigated.[36] The introduction of coumarin moieties in the polymer backbone was found to decrease the oxygen permeability of the noncross-linked composites, while only a slight further decrease was obtained by cross-linking, possibly owing to low cross-link density. Extending this preliminary study, in the present work, we synthesized an EDMA-based copolymer latex with a higher coumarin content, to allow for a higher cross-link density, performed its physicochemical characterization, and studied its cross-linking via [2 + 2] cycloaddition. We then prepared composite films with different weight fractions of hemp nanocellulose, prepared by our group to valorize an abundant local agricultural residue consisting of low-quality bast fibers separated from stalks discarded from plants harvested for oil and seeds.[7] We cross-linked the composites by exposure to UV light to produce insoluble materials, and we finally investigated the properties of the cross-linked composites, with a particular focus on water vapor permeability.

EXPERIMENTAL SECTION

Materials. (4-Methyl)coumarin-7-yl methacrylate (CouMA, Specific Polymers) and sodium dodecyl sulfate (SDS, >99%, Aldrich), potassium persulfate $K_2S_2O_8$ (KPS, ≥99.0%, Aldrich), sodium metabisulfite $Na_2S_2O_5$ (SMBS, 99%, Aldrich), and sodium bicarbonate $NaHCO_3$ (99.7%, Aldrich) were used as received. Deionized water (DI water, 1 μS cm^{-1}) was obtained using a D8 ion exchange demineralizer from A2E Affinage de L'Eau. 2-(2-Methoxy-4-propylphenoxy)ethyl methacrylate (ethoxy dihydroeugenyl methacrylate, EDMA) monomer was synthesized from dihydroeugenol (2-methoxy-4-propylphenol, 98%, Aldrich) as described in a previous work.[37]

Emulsion Copolymerization of EDMA with CouMA. The emulsion copolymerization of EDMA with CouMA (Scheme 1) was carried out in a 50 mL double-walled jacketed glass reactor with a U-shaped glass stirring rod, adapting the procedure previously published for the emulsion polymerization with redox initiation of EDMA monomer;[38] the recipe is summarized in Table 1. The monomer mixture (5.86 g) was prepared by dissolving CouMA (5 wt %) in EDMA; the mixture was purged under argon for 15 min, heating at 40 °C to allow for complete dissolution of CouMA. $K_2S_2O_8$ was dissolved in 9 mL of DI water and placed aside. SDS, $NaHCO_3$, $Na_2S_2O_5$ and the rest of the DI water (27.5 g) were mixed, placed in the reactor, and purged with argon for 30 min (Attention! $Na_2S_2O_5$ and $NaHCO_3$ will produce gas when mixed). The reactor was then heated to 40 °C, and a mixture of monomers was added. Finally, 3 mL of the previously prepared solution of $K_2S_2O_8$ was added in one shot, and this was considered as $t = 0$. The rest of the $K_2S_2O_8$ solution (6 mL) was added over 4 h at 1.5 mL/h, and the polymerization proceeded under mechanical stirring at 200 rpm.

Table 1. Recipe for Redox-Initiated Emulsion Copolymerization of EDMA and CouMA

ingredient	M_w (g/mol)	mass (g)	equivalents	mmol	% wt[a]
EDMA	278.35	5.5670	1.00	20.00	95.00
CouMA	244.25	0.2930	0.06	1.2	5.00
SDS	288.37	0.2344	0.041	0.81	
$K_2S_2O_8$	270.32	0.1172	0.022	0.43	
$Na_2S_2O_5$	190.11	0.1072	0.028	0.56	
$NaHCO_3$	84.00	0.1311	0.078	1.56	
DI water		36.5493			

[a]% weight percent of monomers in the monomer mixture.

Preparation of Hemp Nanocellulose and Nanopaper. An aqueous suspension of hemp nanocellulose (1.3 wt % solid content) was obtained from nonaligned bast fibers from hemp (*Cannabis sativa* L.) plants of the Carmagnola variety following a previously published procedure.[7] The suspension was formed by nanofibrils with lengths of 100−300 nm and widths of 5−12 nm, together with stacks of nanofibrils and larger micron-sized fibers. A handsheet of hemp nanocellulose, indicated below as hemp nanopaper (HNP), with a thickness of 53 μm, was prepared[7] between two precision woven nylon

https://doi.org/10.1021/acssuschemeng.4c01365
ACS Sustainable Chem. Eng. 2024, 12, 8741−8751

screening fabrics using a Rapid-Köthen standard sheet former (Frank-PTI, Germany) and was used as a reference.

Preparation of Poly(EDMA-*co*-CouMA)/Hemp Nanocellulose Composite Films. Hemp nanocellulose was diluted with demineralized water to a solids concentration of 1 wt % by means of a T10 ULTRA-TURRAX homogenizer (IKA-Werke GmbH & Co. KG) at approximately 20k rpm. Then, the desired quantities of hemp nanocellulose suspension were added dropwise to the poly(EDMA-*co*-CouMA) latex while mixing using a magnetic stirrer for 10 min at 1000 rpm. The nanocellulose contents were 15−30−45−60 wt % of nanocellulose (dry weight) with respect to total solids (dry nanocellulose + copolymer). After degassing under a vacuum, the suspensions were cast on Petri dishes lined with a high-density polyethylene (HDPE) film and allowed to dry under ambient conditions until no weight change was detected. The films were then hot-pressed with a PEI LAB 150 P (Pinette Emidecau Industries) press at 80 °C with 2 kN force for 10 min. Part of the composite films was cross-linked by exposure to UV light: a Dymax 2000-EC flood system equipped with a 400 W metal halide lamp (Dymax Corporation) with an emission spectrum in the UVA−UVB range[39] (wavelengths between 280 and 410 nm), was used. The light intensity was fixed at 35 mW cm^{-2} for 20 min at a temperature of about 40 °C. The thicknesses of the obtained composite films ranged from 70 to 95 μm, and within a film, the typical standard deviation for thickness was about 5 μm.

Insoluble Content. A sample of material of about 10 mg was weighed (m_i), wrapped in a metallic mesh, and soaked at room temperature for 24 h in 10 mL of solvent (acetone or toluene). Then, after drying in an oven at 60 °C until a constant weight was reached, the final mass of the sample was recorded (m_f). The insoluble content (%) was calculated as $100 \times \frac{m_f}{m_i}$.

NMR Spectroscopy. ^{1}H-NMR spectroscopy was performed on poly(EDMA-*co*-CouMA) with a Bruker Avance 400 MHz spectrometer at room temperature. The spectra were recorded by dissolving 0.1 mL of sample in 0.5 mL of $CDCl_3$:

^{1}H-NMR spectrum (400 MHz, $CDCl_3$, δ, ppm): 7.40 (m, 1H, **H**-Ar CouMA), 7.26 ($CHCl_3$),7.03 (m, 2H, **H**-Ar CouMA), 6.66 (m, 3H, $\mathbf{H}_{5,3,6}$-Ar), 6.18 (s,1H, **H**-Ar CouMA), 4.10 (m, 4H, O$\mathbf{CH_2}$C$\mathbf{H_2}$OPh), 3.78 (s, 3H, C$\mathbf{H_3}$OPh), 2.45 (t, 2H, $CH_3CH_2C\mathbf{H_2}$Ph), 2.31 ppm (s, 3H, C$\mathbf{H_3}$C=CH_2COO CouMA), 1.85 (m, 2H, OC=OC(CH_3)=C$\mathbf{H_2}\boldsymbol{\alpha,\beta}$), 1.56 (m, 2H, $CH_3C\mathbf{H_2}CH_2$Ph), 0.97 (m, 6H, OC=OC(C$\mathbf{H_3}$)=$CH_2\alpha,\beta$ and C$\mathbf{H_3}CH_2CH_2$Ph).

Fourier Transform Infrared (FTIR) Spectroscopy. Fourier transform infrared (FTIR) spectroscopy was performed in attenuated total reflectance (ATR) mode with a Nicolet iS50 spectrometer (Thermo Fisher Scientific Inc.) fitted with an ATR-Smart Orbit accessory with a diamond crystal. The spectra were taken in the 550−4000 cm^{-1} range, with 32 scans per spectrum and a resolution of 4 cm^{-1}.

Dynamic Light Scattering. A Vasco 3 nanoparticle size analyzer (Cordouan Technologies) was used for performing particle size measurements on the latex by dynamic light scattering (DLS) using the Cumulant model at a temperature of 25 °C. The laser power, time interval, and number of channels were adjusted to obtain a good autocorrelation function. Samples for DLS measurements were prepared by diluting one drop of latex with 5 mL of DI water, and the results are the average of six measurements.

UV−Visible Spectroscopy. UV−visible spectroscopy was performed by means of a JENWAY 6850 UV/vis (Cole-Parmer, UK) UV−visible spectrophotometer in transmission mode. To avoid saturation of the signal, polymer and composite layers, having a thickness of about 10−20 μm, were coated on the side of a quartz cuvette as explained below. The poly(EDMA-*co*-CouMA) latex was dried in an oven at 80 °C and then dissolved in acetone at a 1.5 wt % concentration. A drop of the acetone solution was cast onto the side of a quartz cuvette, and acetone was evaporated in an oven at 40 °C prior to the analysis. Also, composite samples with 15 wt % cellulose were analyzed: the nanocellulose containing latex suspension was further diluted with demineralized water, and then a drop was cast on the side of the cuvette and dried at 80 °C to obtain a composite thin coating. To this aim, the samples were irradiated with UV light using a high-pressure mercury−xenon lamp Lightning Cure LC8 model L9588−02A,[40] equipped with a flexible light guide and optional optical filters, A9616−07 or A9616−11, allowing selecting a specific wavelength range (Hamamatsu Photonics K.K.). To induce the photodimerization of coumarin moieties, favored at wavelengths longer than 300 nm, irradiation was performed either using an A9616−07 filter with a transmittance wavelength of 355−375 nm (λ_{max} = 365 nm, UVA_{365}) or through a polyethylene terephthalate (PET) foil transmitting light above 307 nm (UVA and UVB). To assess the capability of coumarin dimers to revert to their original form, after achieving photodimerization by UVA_{365} light irradiation, the coatings were further irradiated with UVC light using an A9616−11 filter with a transmittance wavelength 230−250 nm (λ_{max} = 248 nm, UVC). The LC8 lamp and filters were manufactured by Hamamatsu. An EIT Powerpuck II radiometer was used to measure the light intensity which was fixed at 36 mW cm^{-2} for UVA irradiation and at 7 mW cm^{-2} for UVC irradiation. UV−vis spectra were obtained after irradiating the samples for given time intervals. The intensity of the absorbance at 318 nm was monitored to assess the extent of the photoreactions.

Differential Scanning Calorimetry. Differential scanning calorimetry (DSC) was carried out by means of a Netzsch DSC 204 F1 Phoenix instrument at a heating/cooling rate of 20 °C min^{-1} under N_2 flux. The temperature range was from −70 to 150 °C for the neat copolymer and −70 to 200 °C for the composites. A heat−cool−heat procedure was performed (with two cooling/heating cycles for the polymers and three cooling/heating cycles for the composites), and the glass transition temperature (T_g) was taken at the inflection point of the glass transition step in the last heating cycle. The data obtained were processed with Netzsch Proteus Analysis software.

Thermogravimetric Analysis with Evolved Gas Analysis. Thermogravimetric analysis with evolved gas analysis (TGA-FTIR) was performed using a NETZSCH TG 209 F1 Libra, increasing the temperature from 25 to 800 °C with a heating rate of 20 °C min^{-1}, under a 20 mL min^{-1} N_2 flux, to prevent thermo-oxidative processes. The first derivative of the residual mass curve (DTG) was calculated to better resolve the main thermal decomposition steps of the analyzed materials with Netzsch Proteus Analysis software. For evolved gas analysis, the TGA was coupled to a Bruker Optics GmbH Tensor II gas IR module.

Scanning Electron Microscopy. Images of the surfaces and freeze-fractured cross-sections of the composite films were taken using a ZEISS SUPRA 40 field-emission scanning electron microscope (FESEM) equipped with a Gemini column (Carl Zeiss S.p.A.), with an acceleration voltage of 3 or 5 kV. Prior to imaging, the samples were coated with platinum to prevent charging.

Wettability. The wettability of the films was investigated by static contact angle measurements performed at room temperature by means of a FTA 1000C instrument (First Ten Ångstroms, Inc.) equipped with a video camera and image analyzer using the sessile drop technique. The probe liquids were water (5 μL drop) and hexadecane (3 μL drop). Several measurements per liquid were performed on each sample by placing the drops in different parts of the sample surface.

Water Vapor Transmission Rate (WVTR). The water vapor permeability of the cross-linked composite films was assessed by means of a PERMATRAN W 3/33 analyzer (Mocon) having a resolution of 0.0001 g m^{-2} day^{-1}. The HNP and a composite film with 30 wt % nanocellulose that was not subjected to cross-linking were also analyzed in the same way for reference. The measurements were performed according to the ASTM F1249−13 standard, and the test conditions were 38 °C ± 1 °C and 50 ± 3 or 90 ± 3% relative humidity (RH). Prior to test, following the ISO 291 standard, the materials were stored at 23 ± 1 °C, 50 ± 2% RH for at least 48 h. The carrier gas was dry nitrogen with a flow of 10 mL min^{-1}, and the exposed sample surface was reduced to 1 cm^2 using aluminum masks: with these conditions, the instrument's measuring range for WVTR is from 0.25 to 500 g m^{-2} day^{-1}. The instantaneous WVTR value was recorded as a function of time; once a steady state was obtained, the WVTR of each material was calculated as the average of the values recorded during 8−10 h. Namely, when the RH was set to 50%, the WVTR was taken as the average of the values between the 40th and 48th h of analysis for samples with

https://doi.org/10.1021/acssuschemeng.4c01365
ACS Sustainable Chem. Eng. 2024, 12, 8741−8751

nanocellulose contents up to 45 wt %, and between the 68th and 78th h of analysis for samples with 60 wt % nanocellulose and for hemp nanopaper (HNP). When the RH was set to 90%, the average WVTR was taken between the 106th and 116th h of analysis. The WVTR values were then normalized to a thickness of 100 μm ($WVTR_{100}$) according to eq 1, where l is the thickness in μm of the tested sample:

$$WVTR_{100} = \frac{WVTR \cdot l}{100} \quad (1)$$

RESULTS AND DISCUSSION

Synthesis and Characterization of Poly(EDMA-*co*-CouMA) Latex. The copolymerization process followed was inspired by previous experiments executed by the team.[36,38] As the previous work showed that eugenol derivatives having double bonds on the side chain gave undesired premature cross-linking,[38] a monomer that has no unsaturation on the alkyl chain, i.e. ethoxy dihydroeugenyl methacrylate (EDMA), was chosen for the copolymerization with the photosensitive comonomer coumarin methacrylate (CouMA). The weight ratio of EDMA to CouMA was set to 95:5 (weight ratios of CouMA higher than 5 wt % could not successfully be solubilized in EDMA at 40 °C). Both eugenol and 7-hydroxy-4-methylcoumarin, the precursors of our methacrylated monomers, are natural molecules.[41,42] The biobased contents of EDMA and CouMA, accounting for the methacrylation of the natural compounds with nonbiobased chemicals, are 63 and 71 wt %, respectively. With the set 95:5 monomer weight ratio, the resulting biobased content of the copolymer is about 63 wt % (see calculation in Table S1). Emulsion polymerization was chosen as the technique to synthesize the polymer due to the sustainability benefits that it could bring to the latex in terms of water as an innocuous continuous phase (no contribution to VOC in the mixture). Using a redox initiation system at a temperature of 40 °C allowed the use of significantly lower energy in comparison to thermal initiation: for most pure acrylates, a conventional latex synthesis is carried out under thermal initiation at 75−90 °C.

The emulsion polymerization of EDMA and CouMA yielded a stable latex of poly(EDMA-*co*-CouMA) at 16 wt % solids content, with a diameter of 53 nm (D_i, intensity-average particle diameter measured by DLS). With the set 5 wt % content of CouMA in the monomer mixture, the expected average molar ratio of EDMA to CouMA moieties in the copolymer (n:m) is about 17:1. From the ^{1}H-NMR spectra, the copolymer structure was confirmed (see Experimental Section and NMR spectrum in Supporting Information, Figure S1), as well as the molar ratio of monomers. Moreover, the methacrylic hydrogens (δ = 5.57 and 6.13 ppm) were absent.

The FTIR spectra of poly(EDMA-*co*-CouMA), and of poly(EDMA) reported as a reference, are shown in Figure 1.

A strong absorption signal was present for both polymers at 1726 cm^{-1} for the stretching of the C═O bonds on the methacrylic backbone; the carbonyl group of coumarin, absorbing at slightly higher wavenumbers, around 1760 cm^{-1}, was visible as a shoulder-only for poly(EDMA-*co*-CouMA). Other absorption characteristics of the coumarin molecule were relatively weak due to the low amount of CouMA units in the copolymer: they were present at 1627 cm^{-1} for C═C stretching in the 3,4 position, 1387 and 982 cm^{-1} for bending and rocking, respectively, of C−H in the 2-pyrone structure.[43]

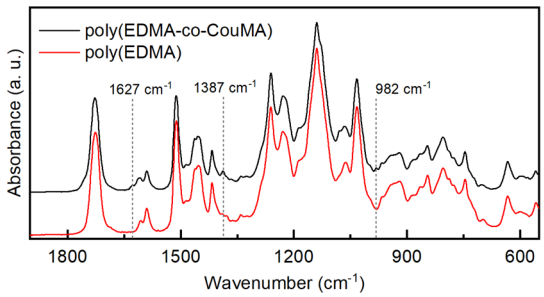

Figure 1. FTIR spectra taken in the ATR mode of poly(EDMA-*co*-CouMA) and of poly(EDMA), and characteristic signals of CouMA are indicated by dashed lines.

The latex was dried at 40 °C to prepare the copolymer films for characterization. However, self-standing films suitable for mechanical and permeability characterization could not be obtained: the copolymer films cracked upon drying or when detached from the substrate. The copolymer was completely soluble in acetone, demonstrating the lack of any significant cross-linking that would lead to the presence of an insoluble fraction (gel content).

The T_g of the copolymer, measured by DSC, was 29 °C, thus slightly higher than the T_g of 25 °C previously found for the homopolymer poly(EDMA), as shown in Figure S2. The introduction of the coumarin derivative in the polymer chain also slightly increased thermal stability, assessed by TGA in a N_2 atmosphere (Figure 2): the $T_{d20\%}$ was 347 °C for poly(EDMA-*co*-CouMA) while it was 334 °C for poly(EDMA); from the DTG (first derivative of the residual mass curve), a main mass loss event was identified with T_{max} = 375 °C for both polymers. The FTIR analysis performed on the evolved volatile products (Figure S3) for poly(EDMA-*co*-CouMA) at T_{max} showed signals in the 3100−2700 cm^{-1} for hydrocarbons, 1800−1660 cm^{-1} for carbonyl functional groups, and distinct signals at 1630, 1609, and 1183 cm^{-1} characteristic of the aromatic and 2-pyrone structures, confirming that this corresponded to the thermal decomposition of the polymer chain. A smaller decomposition event was present above 750 °C where the FTIR spectra of the evolved gas showed the most intense bands in the 2400−2000 cm^{-1} range for CO_2 and CO.

Cross-Linking of Poly(EDMA-*co*-CouMA) via [2 + 2] Photocycloaddition. Coatings cast on the side of quartz cuvettes as explained in the Experimental Section were irradiated with UVA light to induce cross-linking through [2 + 2] photocycloaddition of the coumarin moieties, as depicted in Scheme 2.

The advancement of the cross-linking reaction was followed by UV−visible spectroscopy. The UV−visible spectrum of pristine poly(EDMA-*co*-CouMA) reported in Figure 3a (spectrum at 0 min of irradiation) showed two broad absorption bands in the 250−380 nm region. The band above 300 nm, centered at about 318 nm, absent in the spectrum of poly(EDMA) (Figure S4), is characteristic of the 2-pyrone structure of coumarins, while the band below 300 nm, centered at about 280 nm, is characteristic of $\pi-\pi^*$ transitions of the aromatic structures present in both the CouMA and EDMA moieties.[44,45] The decrease of the intensity of the signal at 318 nm during irradiation with UVA reflects the opening of the 3,4 double bond in the 2-pyrone structure to form the cyclobutane ring when coumarin dimers are formed.[45,46] The photocycloaddition of the coumarin pendant moieties proceeded

https://doi.org/10.1021/acssuschemeng.4c01365
ACS Sustainable Chem. Eng. 2024, 12, 8741−8751

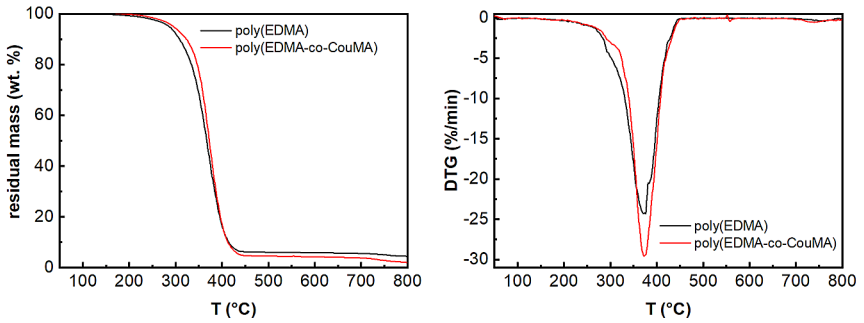

Figure 2. Thermogravimetric analysis of poly(EDMA-*co*-CouMA) compared to poly(EDMA): residual mass vs temperature curves and their first derivative (DTG).

Scheme 2. (a) [2 + 2] Photocycloaddition of Coumarins; (b) Poly(EDMA)-*co*-CouMA Cross-Linked via [2 + 2] Photocycloaddition

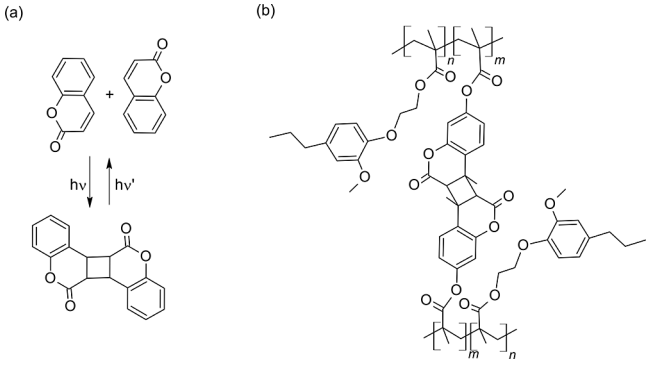

during irradiation with UVA. When the light at 355−375 nm (λ_{max} = 365 nm, UVA_{365}) was used, the coumarin double bond reached almost complete conversion within 180 min (Figure 3a). The possibility to increase the cross-linking reaction rate by irradiation in a wavelength range closer to the absorption maximum of CouMA (318 nm) was also checked: when polychromatic light above 310 nm was used, the conversion was complete already after 20 min (Figure S4).

To assess the possibility to obtain reversion of the [2 + 2] photocycloaddition reaction, latex coatings previously cross-linked via UVA_{365} irradiation were exposed to UVC light (λ_{max} = 248 nm, intensity of 7 mW cm^{-1}). Reversion to the pristine coumarin form was very limited and only detected up to 30 s of UVC irradiation, slightly increasing when the previous irradiation with UVA_{365} had been performed for a relatively short time, e.g., 20 min, thus not reaching complete conversion of CouMA moieties to the dimer form (Figure 4). Continuing

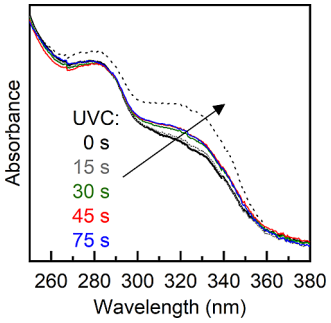

Figure 4. UV−vis spectra of poly(EDMA-*co*-CouMA) film irradiated first with UVA_{365} light with a 36 mW cm^{-2} intensity for 20 min (thick black line) and then with UVC light at a 7 mW cm^{-2} intensity for up to 75 s. The spectrum of the nonirradiated latex film is reported as a reference (dotted line).

the irradiation with UVC for longer times, a degradation phenomenon, also observed for UVC-irradiated poly(EDMA), appeared as indicated by the changes in the UV−vis absorption spectra shown in Figure S4. Indeed, irradiation at 254 nm or shorter wavelengths was reported to lead to photodegradation of polymethacrylate backbones.[47]

While many coumarin derivatives are colored and used as dyes, the coumarin methacrylate used in this work (whose structure is derived from the colorless 7-hydroxy-4-methyl-

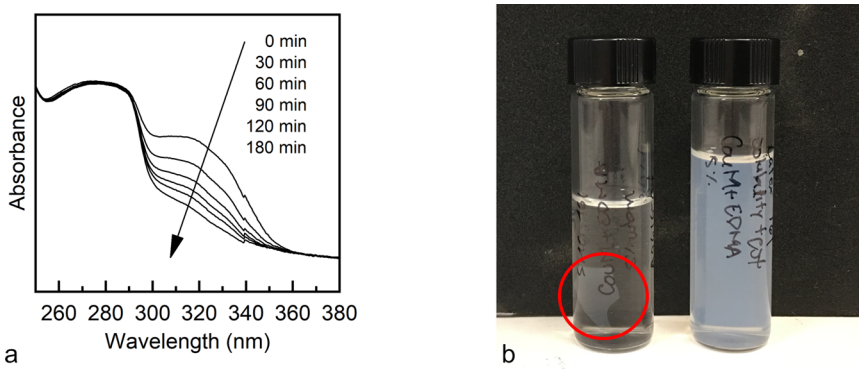

Figure 3. (a) UV−visible spectra of poly(EDMA-*co*-CouMA) latex irradiated with UVA_{365} light with a 36 mW cm^2 intensity for up to 180 min; (b) nonirradiated (right side) and UVA_{365}-irradiated (left side) poly(EDMA-*co*-CouMA) latex films after immersion in acetone: the nonirradiated film was completely soluble while the UVA_{365}-irradiated film remained insoluble as shown in the red circle.

https://doi.org/10.1021/acssuschemeng.4c01365
ACS Sustainable Chem. Eng. 2024, 12, 8741−8751

coumarin) does not show any absorption in the visible part of the spectrum. Thus, its presence did not affect the color of the copolymer, which yielded transparent colorless films. After cross-linking with UVA_{365}, visually, the copolymer films developed a yellowish color, that can be attributed to the formation of coumarin dimers.[48,49] Notably, cross-linking dramatically affected the solubility of the copolymer (as also qualitatively shown in Figure 3b): while the nonirradiated copolymer sample was completely dissolved in acetone (insoluble content was 1−3 wt %), the insoluble content of the copolymer exposed to UVA_{365} irradiation at 36 mW cm^{-2} for 20 min was already 75 wt %, while after 180 min of exposure it was found to be 93 wt %, confirming an efficient cross-linking. On the contrary, the same irradiation treatment did not affect the solubility of the homopolymer poly(EDMA), which was completely soluble in acetone both before and after irradiation.

From DSC analysis, irradiation of the copolymer with UVA_{365} for 180 min resulted in a slight broadening of the glass transition region, with a modest increase of T_g from 29 °C before irradiation to 33 °C after irradiation (see Figure S2). This may indicate that the network formed was quite loose, as expected: in fact, a 5 wt % content of coumarin moieties corresponds to 1 CouMA unit every 17 EDMA units, from which a maximum cross-link density of 10^{-4} mol cm^{-3} may be estimated

A comparison of the thermogravimetric analysis results obtained for the non-irradiated and the irradiated copolymer (Figure S5) showed only minor differences, such as the shift at a slightly higher temperature of the small decomposition event present above 750 °C.

[2 + 2] Photocycloaddition in the Presence of Hemp Nanocellulose. To obtain composites, the copolymer latex was mixed with hemp nanocellulose (FESEM images of the nanocellulose are shown in Figure S6). To monitor the dimerization of the copolymer's CouMA moieties in the presence of the nanocellulose filler, composite coatings, obtained by casting a drop of diluted latex−nanocellulose suspension on quartz slides followed by drying, were subjected to irradiation with UVA_{365} light. The UV−visible spectra were recorded with increasing irradiation times: in Figure 5, the

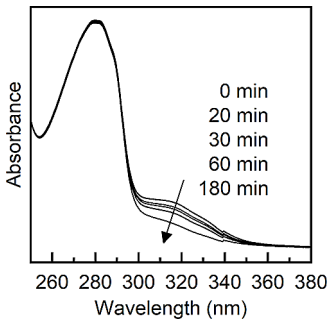

Figure 5. UV−visible spectra of coatings of poly(EDMA-*co*-CouMA) containing 15 wt % of hemp nanocellulose, irradiated with UVA_{365} light for different times.

spectra recorded for the composite with 15 wt % nanocellulose are reported. The dimerization proceeded to high conversion, within similar times as for the filler-free copolymer.

Characterization of Composite Films. Composite films with cellulose contents ranging from 15 to 60 wt % were prepared by simply mixing the latex with the diluted aqueous nanocellulose suspension, casting, and drying in an oven at 40 °C followed by hot pressing at 80 °C. As the cellulosic filler was 100% biobased, the composites had a high biobased content, ranging from 69 to 85 wt % (calculation in Supporting Information, Table S2). The films were self-standing but fragile, particularly at low nanocellulose contents. They were transparent, with a brownish color imparted by the hemp nanocellulose (Figure 6). The colorimetric evaluation of the films is reported in Table S3 together with the experimental parameters adopted for the emasurements.

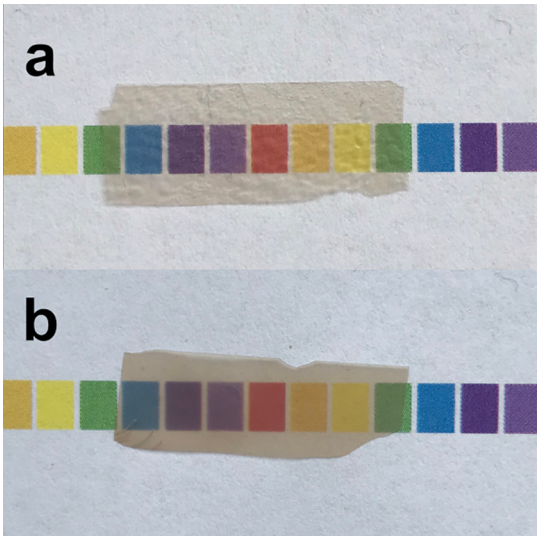

Figure 6. Photos of composites with weight fractions of hemp nanocellulose equal to (a) 30 wt %; (b) 60 wt %.

When the films were irradiated with UV light as described in the Experimental Section to achieve cross-linking, the irradiation caused a yellowing of the composites (see Table S3), reflecting the observed yellowing of the copolymer matrix. The cross-linked composites were completely insoluble in acetone and toluene (insoluble content ≥99 wt %). As nanocellulose is insoluble in acetone, an increase of the insoluble fraction proportional to the cellulose weight fraction is expected for the cross-linked composites with respect to the unfilled cross-linked copolymer. Being the insoluble content of the cross-linked copolymer at around 93 wt % and the cellulose content of the composites in the 15−60 wt % range, insoluble fractions are expected to be between 94 and 97 wt %. However, nanocellulose may physically interact in several ways with the polymer chains and the solvent: the fibril network can either make the polymer less accessible to the solvent or retain the polymer chains through secondary interactions. As a consequence, there is a few percent increase in the insoluble content with respect to the expected value.

The surface of both the uncross-linked and cross-linked composites, observed by FESEM, reflected the morphology of the nanocellulose (Figure S7): fibrils and stacks of fibrils of different dimensions were visible. Comparing the micrographs of uncross-linked and cross-linked composites, a surface morphology change is evident, possibly due to the combined effect of shrinkage of the matrix[50] and microdefect healing upon photodimerization.[51] The observation of freeze-fractured cross-sections of cross-linked composites with 15 and 60 wt % nanocellulose showed that the composites with the highest nanocellulose content had larger porosity (Figure S8).

https://doi.org/10.1021/acssuschemeng.4c01365
ACS Sustainable Chem. Eng. 2024, 12, 8741−8751

The strongest effect of the irradiation on composite films was the change in the water vapor barrier properties. Measurements of WVTR were performed on composites before and after cross-linking, at 38 °C and two different relative humidity (RH) conditions, i.e., 50 and 90%. The WVTR of filler-free copolymer films could not be assessed as defect-free self-standing films suitable for permeability measurements could not be obtained. The WVTR of the HNP at 38 °C and 50% RH was measured and taken as a reference: the value of 167 g m^{-2} day^{-1} measured for the 53 μm-thick handsheet (corresponding to a $WVTR_{100}$ of 89 g m^{-2} day^{-1}) is in the range reported for films made of microfibrillated cellulose (MFC).[52] Indeed, while common paper, obtained from larger cellulose fibers, is highly permeable to water vapor, nanocellulose sheets show, under low RH% conditions (RH < 50%), moderate to low permeability to water vapor, owing to the formation of a tight fibril network through hydrogen bonds, which is however disrupted at high RH%.[53] When measurements were performed on composite films before cross-linking, already at 50% RH their permeability was so high that the WVTR was above the measuring range of the instrument, i.e., 500 g m^{-2} day^{-1}. The barrier properties toward water vapor of the uncross-linked composites were thus much worse than those of reference nanopaper, possibly owing to the presence of submicrometric pinholes (as shown in Figure S7), and measurements at higher RH, where even higher permeability is expected, were not attempted. In contrast, the WVTR of the cross-linked composites was, in all cases, measurable, clearly indicating a positive effect of cross-linking on barrier properties, consistent with the observed microdefect healing. The results obtained for cross-linked composites are summarized in Table 2, where for easier comparison all WVTR values are normalized to a thickness of 100 μm ($WVTR_{100}$) according to eq 1.

Table 2. WVTRs Normalized to a Thickness of 100 μm ($WVTR_{100}$) of Cross-Linked Composites and hemp nanopaper (HNP)

nanocellulose (wt %)	$WVTR_{100}$@ 38 °C 50% RH (g m^{-2} day^{-1})	$WVTR_{100}$@38 °C 90% RH (g m^{-2} day^{-1})
15	18	274
30	22	
45	15	350
60	117	
100 (HNP)	89	

The $WVTR_{100}$ values of the cross-linked films containing up to 45 wt % of cellulose were in the 15−22 g m^{-2} day^{-1} range, therefore lower than that of the HNP taken as a reference, i.e., 89 g m^{-2} day^{-1}. The $WVTR_{100}$ increased to 117, above the value measured for HNP, when the cellulose content was 60 wt %: this abrupt increase may be ascribed to interfacial defects or filler agglomeration appearing at high filler contents. Permeation of water vapor across nanocellulose sheets happens through diffusion in the defective amorphous regions of the fibrils and within the porous structure formed by the fibrils network.[53,54] Our hemp nanocellulose fibrils, as reported in our previous study,[7] have a high degree of crystallinity and thus are mostly impermeable to water vapor. When nanocellulose is dispersed in the polymeric matrix, permeation of the water molecules takes place through the polymer, as well as in the interface regions between polymer and fibrils. The presence of well-dispersed fibrils, as typically achieved at lower cellulose contents, imparts tortuosity to the gas path, decreasing permeability; on the other hand, at high nanocellulose contents, aggregates of fibrils or high matrix-fibril interfacial area, where defects may act as preferential paths for permeation, increase permeability.

When the RH was increased to 90%, the $WVTR_{100}$, measured for the cross-linked composites containing 15 and 45 wt % of nanocellulose, became 15 times and 22 times higher, respectively. Thus, a larger impact of RH on the permeability was confirmed for higher cellulose contents. Notice that this high sensitivity of WVTR to moisture is comparable to what was reported for nanocellulose/PLA composites,[55] and lower than what was found in the case of nanocellulose films.[56,57] The $WVTR_{100}$ values obtained at 50% RH for the films with cellulose contents up to 45 wt % were lower than those reported for other barrier films obtained combining MFC with other polymers, such as starch or beeswax-coated MFC[58] or composites with photocured PEGDA or soybean oil epoxidized acrylate with comparable MFC contents;[59] furthermore, the $WVTR_{100}$ measured at 90% RH, although higher than those reported for PLA and PCL,[60] were lower than, e.g., cellulose acetate or cellulose acetate propionate.[61]

The contact angles of water and hexadecane were measured on the two faces of the composites and on the HNP taken as a reference (Figure 7).

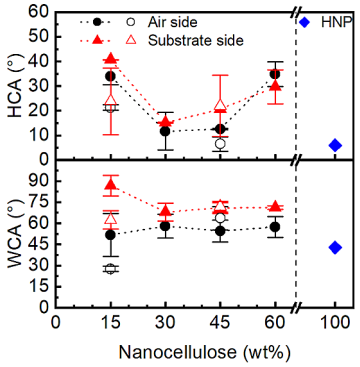

Figure 7. Water (WCA) and hexadecane (HCA) contact angles on the air side and mold side for poly(EDMA-*co*-CouMA)-based composites and for HNP. Full symbols are for uncross-linked composites and hollow symbols for cross-linked composites.

The water and hexadecane contact angles for the HNP were low, as expected, being 43 and 6°, respectively; for each test liquid, similar values were measured on both sides of the film as expected, as the nanopaper was manufactured between two identical nylon cloths. The surface energy was estimated as 57 mN m^{-1}, which is in line with other values reported in the literature for nanocellulose films.[62] The wettabilities of the composites, both before and after irradiation, were affected by the presence of the nonpolar polymer, as well as by that of the SDS surfactant employed for the latex preparation. Notably, the composites were cast on a HDPE-lined open mold; thus, one side of the film was exposed to air during drying (air side) and the other side was in contact with HDPE (substrate side): different values for the WCA were obtained for the air side and the substrate side of the composite films, indicating a preferential arrangement of the components toward one of the sides. On the air side, the contact angle of water was similar for all composites, in the 52−58° range, while on the substrate side, it decreased from 86° for the 15 wt % composite to around 70° for the other composites. For composite with 15 wt %

https://doi.org/10.1021/acssuschemeng.4c01365
ACS Sustainable Chem. Eng. 2024, 12, 8741−8751

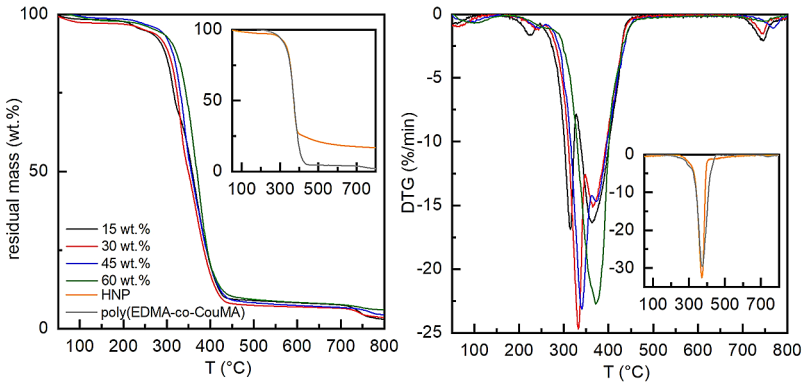

Figure 8. Thermogravimetric analyses of the composites with 15−60 wt % of nanocellulose, and nonfilled poly(EDMA-*co*-CouMA) and hemp nanocellulose handsheet reported as references in the insets: residual mass and first derivative (DTG) of the residual mass curve.

nanocellulose, the variability of the contact angle was larger on the air side (standard deviation of 15°) than on the substrate side (standard deviation of 7°). This large variability was attributed mainly to an inhomogeneous presence of the SDS surfactant at the surface, as confirmed by infrared spectroscopic analysis: characteristic bands of SDS[63,64] i.e., CH_2 asymmetric and symmetric stretching at 2916 and 2849 cm^{-1}, respectively, and S−O asymmetric and symmetric stretching at 1220 and 1080 cm^{-1}, respectively, are very evident in the FTIR spectrum of the air side of the composite film (cf. Figure S9). Surfactants preferentially migrate to the interfaces between substances of very different polarities: in the case of these composites, the interfaces are between the nanocellulose and the polymer and the surface of the film toward air. When nanocellulose concentration is low, the interfacial area between microfibrils and polymer is smaller; thus, a larger amount of surfactant is free to migrate to the surface where it can segregate, forming islands. Indeed the 15 wt % composite showed a larger difference between the WCA on the air side and that on the substrate side than the other composites. Hexadecane contact angles for the composites were always larger than those for the nanopaper and had larger values for the lowest and highest nanocellulose concentrations, on both sides of the composite films.

The thermal analysis of the composites performed by DSC (Figure S2) showed glass transition in the same temperature region as for the unfilled copolymer and, in the first heating cycle only, the characteristic endothermic broad peak corresponding to the evaporation of residual water. No other transitions were detected.

Thermogravimetric analyses were performed on the composites and on the HNP. As for the unfilled copolymer, only minor differences were detectable in the thermograms of the composites after cross-linking with UV light. The results are summarized in Figure 8 for the uncross-linked composites along with the thermograms of the pure copolymer and the nanopaper reported for reference. TGA analyses of cross-linked composites are available in Supporting Information (Figure S10).

The HNP showed only one main weight loss event, at about 360 °C, which is very close to the T_{max} of the copolymer (373 °C). The composite films on the other hand had more complex weight loss patterns. At low temperatures, two small weight losses appeared. The first one around 100 °C may be assigned to the evaporation of residual water, as confirmed by the FTIR spectra of the evolved gas (Figure S3), showing only a broad band above 3300 cm^{-1}, which is characteristic of O−H stretching. A second small weight loss happened between 225 and 250 °C depending on the cellulose contents, consistent with the evaporation of the SDS surfactant: only absorptions at 2932 and 2864 cm^{-1} are evidenced in the FTIR analysis of the evolved volatiles. Two distinct mass losses at temperatures above 300 °C were resolved up to 45 wt % cellulose content. The first main mass loss event was centered at temperatures shifting from 315 to 340 °C with cellulose content increasing from 15 to 45 wt %: it was attributed to the decomposition of nanocellulose. The second main mass loss remained centered around 370 °C for all composites and was attributed to the decomposition of the copolymer matrix. Indeed, at temperatures corresponding to the first main weight loss, i.e., 300−350 °C, the FTIR spectra of the evolved volatile products showed characteristic signals above 3500 cm^{-1} (stretching of O−H), 3100−2600 cm^{-1} (stretching of C−H), 2400−2200 cm^{-1} (CO_2), 1800−1650 cm^{-1} (carbonyl groups), and 1130−1050 cm^{-1} (C−O groups), characteristic of nanocellulose thermal degradation,[65] but lacked the signals at 1640, 1609, and 1583 cm^{-1} characteristic of the aromatic and 2-pyrone structures of the copolymer, which were instead visible in the spectra recorded above 380 °C, following the second main mass loss. The two mass loss events eventually overlapped for the 60 wt % cellulose composite, resulting in one broad peak in the DTG curve centered around 370 °C. The residual masses at 800 °C were not found to increase proportionally to the filler content. A lower thermal stability of nanocellulose at lower weight fractions in composites, as well as a lack of proportionality between cellulose content and residue, has also been reported for PVA-based composites. This has been attributed to the inability of nanocellulose dispersed in a polymer matrix to form the tight network of hydrogen-bonded fibrils that impart high thermal stability to nanocellulose films and promote carbon formation.[66]

CONCLUSIONS

A novel copolymer of ethoxy dihydroeugenyl methacrylate and coumarin methacrylate was synthesized by redox-initiated radical aqueous emulsion polymerization, obtaining a stable latex. The copolymer was characterized by NMR and FTIR, confirming its structure and composition. The presence of the coumarin moieties allowed the cross-linking of the copolymer, by UV irradiation, exploiting the [2 + 2] photocycloaddition reaction. Being waterborne, the copolymer latex could be easily mixed with an aqueous suspension of hemp nanocellulose: composite films containing up to 85 wt % biobased content were obtained using an eco-friendly water-based process, suitable for forming self-standing films. The composites were transparent

https://doi.org/10.1021/acssuschemeng.4c01365
ACS Sustainable Chem. Eng. 2024, 12, 8741−8751

and brownish-colored with good thermal resistance, although fragile, particularly at low nanocellulose contents. Cross-linking of the composites via photocycloaddition was instrumental in achieving water vapor barrier properties: the WVTR of cross-linked films with up to 45 wt % of hemp nanocellulose was reduced 5 times with respect to that of nanopaper obtained from the same nanocellulose. Only when the relative humidity increased from 50 to 90%, permeability increased especially for high cellulose content). With their promising barrier properties and good thermal resistance, these materials could be further developed for application in packaging as an alternative to the current petroleum-based plastics.

■ ASSOCIATED CONTENT

Supporting Information

The Supporting Information is available free of charge at https://pubs.acs.org/doi/10.1021/acssuschemeng.4c01365.

1H NMR spectrum of poly(EDMA-co-CouMA); DSC results; FTIR analyses of evolved gases from TGA of composites; UV−vis spectra of poly(EDMA-co-CouMA) and poly(EDMA) irradiated and nonirradiated; comparison of the thermogravimetric analysis results of composites; morphology of nanocellulose; FESEM images of surfaces of composites; FESEM images of freeze-fractured cross-sections of composites; FTIR spectra of composite films; comparison of the thermogravimetric analysis of composites; biobased content of the composite copolymer; biobased content of the composite films; colorimetric evaluation of composite films; and experimental details of colorimetric evaluation (PDF)

■ AUTHOR INFORMATION

Corresponding Author

Sara Dalle Vacche − *Dipartimento Scienza Applicata e tecnologia, Politecnico di Torino, 10129 Torino, Italy; INSTM-Politecnico di Torino Research Unit, 50121 Firenze, Italy;* orcid.org/0000-0001-5459-5714; Email: sara.dallevacche@polito.it

Authors

Samantha Molina-Gutiérrez − *Dipartimento Scienza Applicata e tecnologia, Politecnico di Torino, 10129 Torino, Italy; ICGM, University Montpellier, 34293 Montpellier, France;* orcid.org/0000-0003-4359-1851

Giuseppe Ferraro − *Dipartimento Scienza Applicata e tecnologia, Politecnico di Torino, 10129 Torino, Italy*

Vincent Ladmiral − *ICGM, University Montpellier, 34293 Montpellier, France;* orcid.org/0000-0002-7590-4800

Sylvain Caillol − *ICGM, University Montpellier, 34293 Montpellier, France;* orcid.org/0000-0003-3106-5547

Patrick Lacroix-Desmazes − *ICGM, University Montpellier, 34293 Montpellier, France;* orcid.org/0000-0002-0197-7062

Yves Leterrier − *Laboratory for Processing of Advanced Composites (LPAC), Ecole Polytechnique Fédérale de Lausanne (EPFL), CH-1015 Lausanne, Switzerland;* orcid.org/0000-0002-0532-0543

Roberta Bongiovanni − *Dipartimento Scienza Applicata e tecnologia, Politecnico di Torino, 10129 Torino, Italy; INSTM-Politecnico di Torino Research Unit, 50121 Firenze, Italy;* orcid.org/0000-0002-2607-9461

Complete contact information is available at: https://pubs.acs.org/10.1021/acssuschemeng.4c01365

Author Contributions

The manuscript was written through the contributions of all authors. All authors have given approval to the final version of the manuscript.

Notes

The authors declare no competing financial interest.

■ ACKNOWLEDGMENTS

The project ComBIOsites has received funding from the European Union's Horizon 2020 research and innovation programme under the Marie Skłodowska-Curie grant agreement No. 789454. Samantha Molina-Gutiérrez thanks the Commission of the European Union for funding her PhD grant through SINCHEM, a Joint Doctorate programme selected under the Erasmus Mundus Action 1 Programme (Framework agreement n° 2013-0037; specific grant agreement n° 532475-EM-5-2017-1-IT-ERAMUNDUS-EPJD). Giuseppe Ferraro acknowledges funding under the National Recovery and Resilience Plan (NRRP), Mission 4 "Education and Research" - Component 2 "From research to business" - Investment 3.1 "Fund for the realization of an integrated system of research and innovation infrastructures" - Call for tender No. n. 3264 of 28/12/2021 of Italian Ministry of Research funded by the European Union − NextGenerationEU - Project code: IR0000027, Concession Decree No. 128 of 21/06/2022 adopted by the Italian Ministry of Research, CUP: B33C22000710006, Project title: iENTRANCE. The authors also thank Loreleï Douard of LGP2 laboratory of the University of Grenoble Alps for assistance in nanocellulose preparation and Miraç Dizman of Politecnico di Torino for colorimetric measurements. The authors thank Elena Rigo for her assistance during the revision of this paper.

■ ABBREVIATIONS

EDMA, ethoxy dihydroeugenyl methacrylate; CouMA, coumarin methacrylate; TGA, thermogravimetric analysis; DSC, differential scanning calorimetry; FTIR, Fourier transform infrared analysis; ATR, attenuated total reflection; NMR, nuclear magnetic resonance; DLS, dynamic light scattering; FESEM, field emission scanning electron microscope; WCA, water contact angle; WVTR, water vapor transmission rate

■ REFERENCES

(1) Kalita, E.; Nath, B. K.; Deb, P.; Agan, F.; Islam, Md. R.; Saikia, K. High Quality Fluorescent Cellulose Nanofibers from Endemic Rice Husk: Isolation and Characterization. *Carbohydr. Polym.* **2015**, *122*, 308−313.

(2) Rashid, S.; Dutta, H. Characterization of Nanocellulose Extracted from Short, Medium and Long Grain Rice Husks. *Ind. Crops Prod.* **2020**, *154*, No. 112627.

(3) Yang, X.; Han, F.; Xu, C.; Jiang, S.; Huang, L.; Liu, L.; Xia, Z. Effects of Preparation Methods on the Morphology and Properties of Nanocellulose (NC) Extracted from Corn Husk. *Ind. Crops Prod.* **2017**, *109*, 241−247.

(4) Hu, L.; Du, H.; Liu, C.; Zhang, Y.; Yu, G.; Zhang, X.; Si, C.; Li, B.; Peng, H. Comparative Evaluation of the Efficient Conversion of Corn Husk Filament and Corn Husk Powder to Valuable Materials via a Sustainable and Clean Biorefinery Process. *ACS Sustain. Chem. Eng.* **2019**, *7* (1), 1327−1336.

(5) Dai, D.; Fan, M.; Collins, P. Fabrication of Nanocelluloses from Hemp Fibers and Their Application for the Reinforcement of Hemp Fibers. *Ind. Crops Prod.* **2013**, *44*, 192−199.

(6) Agate, S.; Tyagi, P.; Naithani, V.; Lucia, L.; Pal, L. Innovating Generation of Nanocellulose from Industrial Hemp by Dual Asymmetric Centrifugation. *ACS Sustain. Chem. Eng.* **2020**, *8* (4), 1850−1858.
(7) Dalle Vacche, S.; Karunakaran, V.; Patrucco, A.; Zoccola, M.; Douard, L.; Ronchetti, S.; Gallo, M.; Schreier, A.; Leterrier, Y.; Bras, J.; Beneventi, D.; Bongiovanni, R. Valorization of Byproducts of Hemp Multipurpose Crop: Short Non-Aligned Bast Fibers as a Source of Nanocellulose. *Molecules* **2021**, *26* (16), 4723.
(8) Aulin, C.; Gällstedt, M.; Lindström, T. Oxygen and Oil Barrier Properties of Microfibrillated Cellulose Films and Coatings. *Cellulose* **2010**, *17* (3), 559−574.
(9) Poothanari, M. A.; Schreier, A.; Missoum, K.; Bras, J.; Leterrier, Y. Photocured Nanocellulose Composites: Recent Advances. *ACS Sustain. Chem. Eng.* **2022**, *10* (10), 3131−3149.
(10) Tehfe, M.; Louradour, F.; Lalevée, J.; Fouassier, J.-P. Photopolymerization Reactions: On the Way to a Green and Sustainable Chemistry. *Appl. Sci.* **2013**, *3* (2), 490−514.
(11) Bongiovanni, R.; Vacche, S. D.; Vitale, A. Photoinduced Processes as a Way to Sustainable Polymers and Innovation in Polymeric Materials. *Polymers* **2021**, *13* (14), 2293.
(12) Pierau, L.; Elian, C.; Akimoto, J.; Ito, Y.; Caillol, S.; Versace, D.-L. Bio-Sourced Monomers and Cationic Photopolymerization: The Green Combination towards Eco-Friendly and Non-Toxic Materials. *Prog. Polym. Sci.* **2022**, *127*, No. 101517.
(13) Voet, V. S. D.; Guit, J.; Loos, K. Sustainable Photopolymers in 3D Printing: A Review on Biobased, Biodegradable, and Recyclable Alternatives. *Macromol. Rapid Commun.* **2021**, *42* (3), No. 2000475.
(14) Lebedevaite, M.; Ostrauskaite, J.; Skliutas, E.; Malinauskas, M. Photoinitiator Free Resins Composed of Plant-Derived Monomers for the Optical μ-3D Printing of Thermosets. *Polymers* **2019**, *11* (1), 116.
(15) Calvino, C. Photocycloadditions for the Design of Reversible Photopolymerizations. *CHIMIA* **2022**, *76* (10), 816−816.
(16) Mariano, M.; El Kissi, N.; Dufresne, A. Cellulose Nanocrystals and Related Nanocomposites: Review of Some Properties and Challenges. *J. Polym. Sci., Part B: Polym. Phys.* **2014**, *52* (12), 791−806.
(17) Ansari, F.; Galland, S.; Johansson, M.; Plummer, C. J. G.; Berglund, L. A. Cellulose Nanofiber Network for Moisture Stable, Strong and Ductile Biocomposites and Increased Epoxy Curing Rate. *Compos. Part Appl. Sci. Manuf.* **2014**, *63*, 35−44.
(18) Rigo, E.; Ladmiral, V.; Caillol, S.; Lacroix-Desmazes, P. Recent Advances in Radical Polymerization of Bio-Based Monomers in Aqueous Dispersed Media. *RSC Sustain.* **2023**, *1* (4), 788−813.
(19) Zhang, L.; Ma, J.; Lyu, B.; Zhang, Y.; Thakur, V. K.; Liu, C. A Sustainable Waterborne Vanillin−Eugenol−Acrylate Miniemulsion with Suitable Antibacterial Properties as a Substitute for the Styrene−Acrylate Emulsion. *Green Chem.* **2021**, *23* (19), 7576−7588.
(20) Alexakis, A. E.; Ayyachi, T.; Mousa, M.; Olsén, P.; Malmström, E. 2-Methoxy-4-Vinylphenol as a Biobased Monomer Precursor for Thermoplastics and Thermoset Polymers. *Polymers* **2023**, *15* (9), 2168.
(21) Mahajan, M. S.; Gite, V. V. Self-Healing Polyurethane Coatings of Eugenol-Based Polyol Incorporated with Linseed Oil Encapsulated Cardanol-Formaldehyde Microcapsules: A Sustainable Approach. *Prog. Org. Coat.* **2022**, *162*, No. 106534.
(22) Polunin, Y.; Burns, T. J.; Serum, E. M.; Sibi, M. P.; Voronov, A. Evaluation of 3-Allyl-5-Vinylveratrole in Latex Copolymerization with an Acrylic Monomer from High Oleic Soybean Oil. *ACS Sustain. Chem. Eng.* **2021**, *9* (20), 7003−7011.
(23) Ladmiral, V.; Jeannin, R.; Fernandes Lizarazu, K.; Lai-Kee-Him, J.; Bron, P.; Lacroix-Desmazes, P.; Caillol, S. Aromatic Biobased Polymer Latex from Cardanol. *Eur. Polym. J.* **2017**, *93*, 785−794.
(24) Li, W. S. J.; Negrell, C.; Ladmiral, V.; Lai-Kee-Him, J.; Bron, P.; Lacroix-Desmazes, P.; Joly-Duhamel, C.; Caillol, S. Cardanol-Based Polymer Latex by Radical Aqueous Miniemulsion Polymerization. *Polym. Chem.* **2018**, *9* (18), 2468−2477.
(25) Molina-Gutiérrez, S.; Li, W. S. J.; Perrin, R.; Ladmiral, V.; Bongiovanni, R.; Caillol, S.; Lacroix-Desmazes, P. Radical Aqueous Emulsion Copolymerization of Eugenol-Derived Monomers for Adhesive Applications. *Biomacromolecules* **2020**, *21* (11), 4514−4521.
(26) Sarker, S. D.; Nahar, L. Progress in the Chemistry of Naturally Occurring Coumarins. In *Progress in the Chemistry of Organic Natural Products 106*; Kinghorn, A. D., Falk, H., Gibbons, S., Kobayashi, J., Eds.; Progress in the Chemistry of Organic Natural Products; Springer International Publishing: Cham, 2017; 241−304.
(27) Ciamician, G.; Silber, P. Chemische Lichtwirkungen. *Berichte Dtsch. Chem. Ges.* **1902**, *35* (4), 4128−4131.
(28) Cazin, I.; Rossegger, E.; Guedes de la Cruz, G.; Griesser, T.; Schlögl, S. Recent Advances in Functional Polymers Containing Coumarin Chromophores. *Polymers* **2021**, *13* (1), 56.
(29) Liu, X.; Yi, C.; Zhu, Y.; Yang, Y.; Jiang, J.; Cui, Z.; Jiang, M. Pickering Emulsions Stabilized by Self-Assembled Colloidal Particles of Copolymers of P(St-Alt-MAn)-Co-P(VM-Alt-MAn). *J. Colloid Interface Sci.* **2010**, *351* (2), 315−322.
(30) Abdollahi, A.; Roghani-Mamaqani, H.; Herizchi, A.; Alidaei-Sharif, H.; Enayati, A.; Sajedi-Amin, S. Light-Induced Spherical to Dumbbell-like Morphology Transition of Coumarin-Functionalized Latex Nanoparticles by a $[2\pi + 2\pi]$ Cycloaddition Reaction: A Fast and Facile Strategy to Anisotropic Geometry. *Polym. Chem.* **2020**, *11* (12), 2053−2069.
(31) Li, H.; Zhou, J.; Zhao, J. Fabrication of Dual-Functional Cellulose Nanocrystals/Fluorinated Polyacrylate Containing Coumarin Derivatives by RAFT-Assisted Pickering Emulsion Polymerization for Self-Healing Application. *Appl. Surf. Sci.* **2023**, *614*, No. 156180.
(32) Zhou, J.; Liu, X.; Wang, X. Photo-Responsive Cellulose Nanocrystal Modified Fluorinated Polyacrylate Based on Coumarin Chemistry. *J. Appl. Polym. Sci.* **2023**, *140* (16), No. e53757.
(33) Zhou, J.; Wang, X.; Liu, X.; Li, X. Design and Synthesis of Waterborne Light-Responsive Cellulose Nanocrystal/Fluorinated Polyacrylate Films toward Oil/Water Repellent and Self-Healing Properties. *Cellulose* **2022**, *29* (14), 7703−7720.
(34) Wong, C. S.; Hassan, N. I.; Su'ait, M. S.; Pelach Serra, M. A.; Mendez Gonzalez, J. A.; Granda, L. A.; Badri, K. H. Photo-Activated Self-Healing Bio-Based Polyurethanes. *Ind. Crops Prod.* **2019**, *140*, No. 111613.
(35) Qiu, Y.; Munna, D.-R.; Wang, F.; Xi, J.; Wang, Z.; Wu, D. Regulating Asynchronous Deformations of Biopolyester Elastomers via Photoprogramming and Strain-Induced Crystallization. *Macromolecules* **2021**, *54* (12), 5694−5704.
(36) Dalle Vacche, S.; Molina-Gutierrez, S.; Ladmiral, V.; Caillol, S.; Lacroix-Desmazes, P.; Bongiovanni, R. Photochemical [2 + 2] Cycloaddition of Biobased Latexes for Composites with Microfibrillated Cellulose. *Chem. Eng. Trans.* **2022**, *92*, 277−282.
(37) Molina-Gutiérrez, S.; Manseri, A.; Ladmiral, V.; Bongiovanni, R.; Caillol, S.; Lacroix-Desmazes, P. Eugenol: A Promising Building Block for Synthesis of Radically Polymerizable Monomers. *Macromol. Chem. Phys.* **2019**, *220* (14), No. 1900179.
(38) Molina-Gutiérrez, S.; Ladmiral, V.; Bongiovanni, R.; Caillol, S.; Lacroix-Desmazes, P. Emulsion Polymerization of Dihydroeugenol-, Eugenol-, and Isoeugenol-Derived Methacrylates. *Ind. Eng. Chem. Res.* **2019**, *58* (46), 21155−21164.
(39) *Dymax 2000-PC and 5000-PC UV Light Curing Flood Systems*. https://www.uvpacific.com.au/wp-content/uploads/2013/09/lit206eu_2000_pc_5000_pc_uv_curing_flood_lamps_sg.pdf (accessed 2024−04−15).
(40) *LIGHTNINGCURE Spot light source LC8 Hamamatsu Photonics Datasheet*. https://www.hamamatsu.com/content/dam/hamamatsu-photonics/sites/documents/99_SALES_LIBRARY/etd/LC8_TLSZ1008E.pdf (accessed 2024−04−11).
(41) Morales-Cerrada, R.; Molina-Gutierrez, S.; Lacroix-Desmazes, P.; Caillol, S. Eugenol, a Promising Building Block for Biobased Polymers with Cutting-Edge Properties. *Biomacromolecules* **2021**, *22* (9), 3625−3648.
(42) Vitale, D. L.; Icardi, A.; Rosales, P.; Spinelli, F. M.; Sevic, I.; Alaniz, L. D. Targeting the Tumor Extracellular Matrix by the Natural Molecule 4-Methylumbelliferone: A Complementary and Alternative Cancer Therapeutic Strategy. *Front. Oncol.* **2021**, *11*, No. 710061.

https://doi.org/10.1021/acssuschemeng.4c01365
ACS Sustainable Chem. Eng. 2024, 12, 8741−8751

(43) Kuş, N.; Breda, S.; Reva, I.; Tasal, E.; Ogretir, C.; Fausto, R. FTIR Spectroscopic and Theoretical Study of the Photochemistry of Matrix-Isolated Coumarin. *Photochem. Photobiol.* **2007**, *83* (5), 1237−1253.
(44) Fu, Q.; Cheng, L.; Zhang, Y.; Shi, W. Preparation and Reversible Photo-Crosslinking/Photo-Cleavage Behavior of 4-Methylcoumarin Functionalized Hyperbranched Polyester. *Polymer* **2008**, *49* (23), 4981−4988.
(45) Seoane-Rivero, R.; Ruiz-Bilbao, E.; Navarro, R.; Laza, J. M.; Cuevas, J. M.; Artetxe, B.; Gutiérrez-Zorrilla, J. M.; Vilas-Vilela, J. L.; Marcos-Fernandez, Á. Structural Characterization of Mono and Dihydroxylated Umbelliferone Derivatives. *Molecules* **2020**, *25* (15), 3497.
(46) Trenor, S. R.; Long, T. E.; Love, B. J. Development of a Light-Deactivatable PSA Via Photodimerization. *J. Adhes.* **2005**, *81* (2), 213−229.
(47) Shanti, R.; Hadi, A. N.; Salim, Y. S.; Chee, S. Y.; Ramesh, S.; Ramesh, K. Degradation of Ultra-High Molecular Weight Poly(Methyl Methacrylate- Co -Butyl Acrylate- Co -Acrylic Acid) under Ultra Violet Irradiation. *RSC Adv.* **2017**, *7* (1), 112−120.
(48) Wang, H.-J.; Zhang, H.-Y.; Xing, W.-W.; Wu, H.; Cui, Y.-L.; Liu, Y. Photodimerization-Induced Transition of Helixes to Vesicles Based on Coumarin-12-Crown-4. *Chin. Chem. Lett.* **2022**, *33* (8), 4033−4036.
(49) Anet, R. The Photodimers of Coumarin and Related Compounds. *Can. J. Chem.* **1962**, *40* (7), 1249−1257.
(50) Shi, D.; Matsusaki, M.; Kaneko, T.; Akashi, M. Photo-Cross-Linking and Cleavage Induced Reversible Size Change of Bio-Based Nanoparticles. *Macromolecules* **2008**, *41* (21), 8167−8172.
(51) Abdallh, M.; Hearn, M. T. W.; Simon, G. P.; Saito, K. Light Triggered Self-Healing of Polyacrylate Polymers Crosslinked with 7-Methacryloyoxycoumarin Crosslinker. *Polym. Chem.* **2017**, *8* (38), 5875−5883.
(52) Rodionova, G.; Lenes, M.; Eriksen, Ø.; Gregersen, Ø. Surface Chemical Modification of Microfibrillated Cellulose: Improvement of Barrier Properties for Packaging Applications. *Cellulose* **2011**, *18* (1), 127−134.
(53) Nair, S. S.; Zhu, J.; Deng, Y.; Ragauskas, A. J. High Performance Green Barriers Based on Nanocellulose. *Sustain. Chem. Process.* **2014**, *2* (1), 23.
(54) Solhi, L.; Guccini, V.; Heise, K.; Solala, I.; Niinivaara, E.; Xu, W.; Mihhels, K.; Kröger, M.; Meng, Z.; Wohlert, J.; Tao, H.; Cranston, E. D.; Kontturi, E. Understanding Nanocellulose−Water Interactions: Turning a Detriment into an Asset. *Chem. Rev.* **2023**, *123* (5), 1925−2015.
(55) Song, Z.; Xiao, H.; Zhao, Y. Hydrophobic-Modified Nano-Cellulose Fiber/PLA Biodegradable Composites for Lowering Water Vapor Transmission Rate (WVTR) of Paper. *Carbohydr. Polym.* **2014**, *111*, 442−448.
(56) Lu, P.; Xiao, H.; Pan, Y. Improving Water Vapor Barrier of Green-Based Nanocellulose Film via Hydrophobic Coating. In *Materials Science and Energy Engineering (CMSEE 2014)*; World Scientific, 2015; 148−153.
(57) Fernández-Santos, J.; Valls, C.; Cusola, O.; Roncero, M. B. Improving Filmogenic and Barrier Properties of Nanocellulose Films by Addition of Biodegradable Plasticizers. *ACS Sustain. Chem. Eng.* **2021**, *9* (29), 9647−9660.
(58) Spence, K. L.; Venditti, R. A.; Rojas, O. J.; Pawlak, J. J.; Hubbe, M. A. WATER VAPOR BARRIER PROPERTIES OF COATED AND FILLED MICROFIBRILLATED CELLULOSE COMPOSITE FILMS. *BioResources* **2011**, *6* (4), 4370−4388.
(59) Amior, A.; Satha, H.; Vitale, A.; Bongiovanni, R.; Dalle Vacche, S. Photocured Composite Films with Microfibrillated Cellulose: A Study of Water Vapor Permeability. *Coatings* **2023**, *13* (2), 297.
(60) Duan, Z.; Thomas, N. L. Water Vapour Permeability of Poly(Lactic Acid): Crystallinity and the Tortuous Path Model. *J. Appl. Phys.* **2014**, *115* (6), No. 064903.
(61) Shogren, R. Water Vapor Permeability of Biodegradable Polymers. *J. Environ. Polym. Degrad.* **1997**, *5* (2), 91−95.
(62) Zhu, H.; Narakathu, B. B.; Fang, Z.; Aijazi, A. T.; Joyce, M.; Atashbar, M.; Hu, L. A Gravure Printed Antenna on Shape-Stable Transparent Nanopaper. *Nanoscale* **2014**, *6* (15), 9110−9115.
(63) Scheuing, D. R.; Weers, J. G. A Fourier Transform Infrared Spectroscopic Study of Dodecyltrimethylammonium Chloride/Sodium Dodecyl Sulfate Surfactant Mixtures. *Langmuir* **1990**, *6* (3), 665−671.
(64) Hafizah, M. A. E.; Riyadi, A. F.; Manaf, A.; Andreas. Particle Size Reduction of Polyaniline Assisted by Anionic Emulsifier of Sodium Dodecyl Sulphate (SDS) Through Emulsion Polymerization. *IOP Conf. Ser. Mater. Sci. Eng.* **2019**, *515* (1), No. 012080.
(65) Quiévy, N.; Jacquet, N.; Sclavons, M.; Deroanne, C.; Paquot, M.; Devaux, J. Influence of Homogenization and Drying on the Thermal Stability of Microfibrillated Cellulose. *Polym. Degrad. Stab.* **2010**, *95* (3), 306−314.
(66) Rowe, A. A.; Tajvidi, M.; Gardner, D. J. Thermal Stability of Cellulose Nanomaterials and Their Composites with Polyvinyl Alcohol (PVA). *J. Therm. Anal. Calorim.* **2016**, *126* (3), 1371−1386.

https://doi.org/10.1021/acssuschemeng.4c01365
ACS Sustainable Chem. Eng. 2024, 12, 8741−8751